

# An *ab initio* molecular dynamics study of varied compositions of the LiF-NaF-KF molten salt

Veronica Heyl<sup>a</sup>, Benjamin Beeler<sup>a,b</sup>

<sup>a</sup>*North Carolina State University, Raleigh, 27607, NC, USA*

<sup>b</sup>*Idaho National Laboratory, Idaho Falls, 83415, ID, USA*

---

## Abstract

With increasing interest in molten salt reactors, there becomes a demand for investigations into thermophysical properties of salt systems. The LiF-NaF-KF (FLiNaK) salt system is a primary candidate for use in these reactors. However, the thermophysical properties of compositions outside the eutectic composition are still largely unknown. In this article, properties of ten unique compositions, including four ternary compositions, are investigated using *ab initio* molecular dynamics simulations across five temperatures between 900 K and 1300 K. The properties of interest are the density, thermal expansion, bulk modulus, compressibility, heat capacity, and enthalpy of mixing. In general, the results were found to be in good agreement with other literature and experimental results. The density and heat capacity had a tendency to be slightly underpredicted. No conclusions could be drawn about the bulk modulus and compressibility in terms of compositional dependence. The thermal expansion had a negative trend with respect to the LiF concentration and no trends were observed for the NaF or KF concentration. The enthalpy of mixing shows minima for the ternary compositions, with the near-equiautomic composition exhibiting the lowest values. This work shows the potential for compositional tailoring in the FLiNaK system to optimize thermophysical properties.

*Keywords:* molten salts, thermophysical properties, AIMD, FLiNaK

---

## 1. Introduction

Molten salts are ionic liquid mixtures at high temperatures with high heat capacity and thermal conductivity. These properties make molten salts useful as a coolant or fuel salt for molten salt reactors (MSRs). Research into MSRs was largely neglected after the experiments by Oak Ridge National Laboratory during the late 1960s[1]. The advantages of an MSR compared to solid fuel reactors are that MSRs do not need traditional fuel fabrication, possess increased intrinsic safety, and have a high working temperature[2]. Because of their benefits, there has been renewed interest in MSRs in the past few years. With this comes the need to characterize molten salts and determine their thermophysical properties, which are required to parameterize complex fluid dynamics and chemical interaction models[1, 3].

The LiF-NaF-KF (FLiNaK) salt system is one of the primary candidates to operate as a coolant salt in MSRs. FLiNaK has been proposed as the heat transfer medium in the Very High-Temperature Reactor, a graphite-moderated, gas-cooled Generation IV concept reactor[4], and is of interest to serve as the primary coolant in MSRE-type designs. FLiNaK

is also often utilized as a surrogate for LiF-BeF<sub>2</sub> (FLiBe), which is also of interest in MSRs, but more challenging to explore experimentally due to the toxicity of Be. The volumetric heat capacity for FLiNaK is similar to water but without the issue of critical heat flux due to the large margin to boiling. Additionally, FLiNaK can operate under ambient pressure conditions, allowing for the removal of the high system pressure in water-cooled reactors [5]. Thus, a significant amount of experimental research has been performed on FLiNaK to determine select thermophysical and chemical properties.

Frandsen et al. investigated the density as a function of temperature between approximately 500°C and 1500°C, the total scattering structure function, and the pair distribution function of the eutectic composition[6]. Anderson et al. collaborated with Oak Ridge National Laboratory to determine the density, equilibrium volume, coefficient of thermal expansion, self-diffusion coefficients for constituent ions at 973 K, 1223 K, and 1423 K, and the self-diffusion coefficient for solute ions at 973 K[7]. All of these properties were determined at the eutectic composition. Liu et al. studied the microstructures of lutetium fluoride and oxyfluoride structures in eutectic FLiNaK using Raman spectroscopy and density functional theory[8]. Ambrosek et al. used previously acquired experimental data to determine the heat transfer of the eutectic composition in comparison to the Dittus-Boelter correlation[5]. Additional experiments have been performed on the eutectic composition [9, 10, 11].

Thermophysical properties are difficult to determine experimentally because of the toxicity of salts, the targeted high temperatures, and the cost of the experiment [1]. In lieu of an abundance of high-fidelity experimental data, a computational approach can be pursued to complement and supplement the existing experimental data. Salanne et al. constructed interatomic potentials for mixtures of LiF, NaK, KF, and ZrF<sub>4</sub> and used them for molecular dynamics simulations to evaluate the heat-transfer properties of FLiNaK and NaF-ZrF<sub>4</sub>[12]. Lee et al. used molecular dynamics to train neural network forcefields and reparametrized analytical forcefields in order to use large-scale molecular dynamics in the determination of structural and transport properties[13]. Sona et al. used computational fluid dynamics simulations to investigate the flow and heat transfer characteristics of eutectic FLiNaK[14]. Recently, *ab initio* molecular dynamics simulations (AIMD) have begun to be explored to determine thermophysical properties, structure, and speciation in FLiNaK[15, 6, 16, 17].

The common trend among previous works is the selection of investigating only the eutectic composition. As most experimental work has been done on this composition, previous computational work purposely and appropriately chose to focus on the composition that had data available for comparison. While understandable, due to corrosion, changing redox potential, and other variables in a reactor environment, the composition of the salt may slightly change as a function of time. Additionally, while the eutectic composition has the minimum melting point for this ternary system, there may be other properties (density, viscosity, heat capacity, etc.) that are more beneficial at non-eutectic compositions, but which are largely unknown[4]. While both thermophysical and transport properties are required for the correct implementation of molten salts in a reactor system, the initial evaluation of thermophysical properties, which are more easily obtainable through both experimental and computational efforts [18, 19, 20], provides an initial step in the full property evaluation of key molten salt systems. Thus, only thermophysical properties are the focus of this manuscript.

This work seeks to more fully characterize the thermophysical properties of FLiNaK through a first principles computational investigation of four ternary compositions (includ-

60 ing the eutectic), three binary eutectic compositions, and three pure alkali-halide salt con-  
61 stituents. The density, bulk modulus, compressibility, heat capacity, thermal expansion, and  
62 enthalpy of mixing for each different composition in the FLiNaK system will be determined  
63 using appropriate temperatures between 900 K and 1300 K. This is the most extensive in-  
64 vestigation of thermophysical properties across the compositional and temperature regimes  
65 in the nuclear-relevant molten salt FLiNaK.

## 66 2. Computational Methods

67 Ten unique compositions (all compositions are stated in mole percent) were studied for  
68 the LiF-NaF-KF salt system, including four ternary compositions (eutectic 46-12-42, 16-  
69 42-42, 32-34-34, and 42-42-16), three binary eutectic compositions (0-40-60, 51-0-49, and  
70 61-39-0), and the three pure alkali-halide salt constituents (LiF, NaF, and KF). The initial  
71 structure was prepared by inserting the respective molecules into a supercell via the Packmol  
72 package [21], with 100 atoms for the ternary systems and 200 atoms for all other systems.  
73 Such system sizes have been shown to produce converged and comparable results for AIMD  
74 analyses of molten salts [22, 23]. AIMD simulations were performed using the Vienna *ab*  
75 *initio* Simulation Package (VASP)[24, 25, 26]. The temperature range investigated for each  
76 composition depended upon the corresponding melting point of that composition, with the  
77 ternary system temperatures ranging from 900 K to 1300 K, binary system temperatures  
78 from 1000 K to 1300 K, and the pure constituent temperatures from 1100 K to 1300 K. The  
79 energy cutoff was 600 eV, which is 100 eV higher than the recommended maximum for the  
80 pseudopotentials utilized, and the electronic optimization criterion was  $10^{-3}$  eV. Convergence  
81 testing was performed with more fine energy convergence criteria to ensure that the results  
82 were not affected by the choice of electronic optimization. A  $1 \times 1 \times 1$  k-point mesh was used,  
83 as this has been shown to be sufficient in prior simulations for molten salts with similarly  
84 sized supercells[18, 15]. The vdW-DF2 van der Waals functional was used to account for the  
85 dispersion interactions[27, 28]. While there are many choices of dispersion interactions avail-  
86 able within VASP, this specific choice was made due to its ability to replicate the properties  
87 of various chloride salts[18]. A brief examination of the DFT-D3 dispersion correction term  
88 [29] was also explored, which did not show superior predictions.

89 In the Open Visualization Tool (OVITO)[30], the initial structures were verified to have  
90 no bonds shorter than 1.5 Å, indicating a reasonable initial guess. The structures were  
91 equilibrated using VASP at each temperature studied. The initial equilibrium simulation for  
92 each composition occurred at 1100 K. The energy was evaluated versus time to check if the  
93 system was equilibrated. If the slope of the running average was approximately zero, the  
94 structure was considered to be at equilibrium. If not, the simulation was continued until it  
95 was determined that equilibrium was reached. Typically, equilibration takes approximately  
96 10-15 ps.

97 Utilizing the equilibrated structures, the system was further evolved at different specified  
98 volumes to obtain the pressure as a function of volume. The systems were equilibrated for a  
99 further 4 ps, with time-averaging to determine the energy and pressure over the final 3 ps.  
100 At least six data points were included for each composition and temperature, ensuring that  
101 the pressures ranged from -2 to +10 kbar, with at least one pressure greater than 5 kbar.  
102 This is in accordance with a prior procedure utilized[18]. Five simulations were performed

for each unique volume for statistical significance. Thus, for a given composition and temperature, approximately thirty simulations were performed. The pressure as a function of the volume, shown in fig. 1a, was determined by fitting a quadratic equation, allowing for the determination of the volume at which the pressure is zero.

The zero pressure volume, along with the mass, was used to calculate the density. The parabolic fit of the volume-pressure curve was used to calculate the bulk modulus and compressibility:

$$K = -V \left( \frac{\partial P}{\partial V} \right)_{P=0} = \frac{1}{\beta} \quad (1)$$

where K is the bulk modulus, V is the volume, P is the pressure, and  $\beta$  is the compressibility.

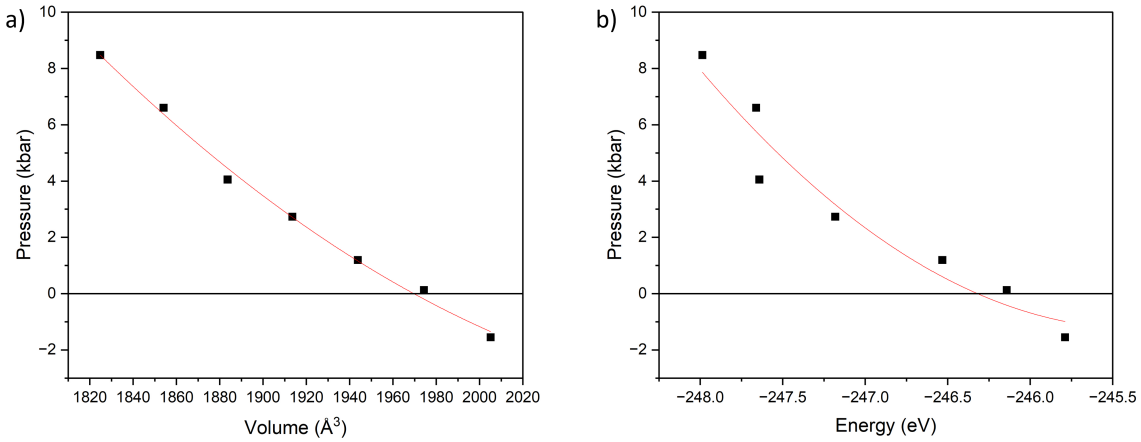


Figure 1: An example of the a) pressure as a function of volume and b) pressure as a function of energy for the 16-42-42 mol% composition at 1000 K.

In a similar manner used to determine the density, the heat capacity can also be found. The pressure as a function of potential energy, shown in fig. 1b, was determined by fitting a quadratic equation, allowing for the determination of the potential energy at which the pressure is zero. This zero-pressure potential energy is then added to the kinetic energy, and the total energy is plotted versus temperature. A linear function is fit to the data to obtain the total energy as a function of temperature. From this, the heat capacity can be determined:

$$C_p = \lim_{\Delta T \rightarrow 0} \frac{\partial E}{\partial T} \quad (2)$$

where  $C_p$  is the heat capacity, T is the absolute temperature, and E is the total energy. It was verified that a linear function adequately represented the data, indicating a constant heat capacity over the temperature range investigated.

The thermal expansion is determined by analyzing the zero-pressure volume as a function of temperature, treating the coefficient of thermal expansion ( $\alpha$ ) as:

$$\alpha = \frac{1}{V_0} \left( \frac{\partial V}{\partial T} \right)_p \quad (3)$$

123 where  $V_0$  is a reference volume at the lowest temperature explored for each composition.

124 The enthalpy of mixing is determined from the potential energy of the mixed system and  
125 the three binary salts:

$$\Delta H^{mix} = \frac{E_{ABC}}{M_{ABC}} - \frac{x_A E_A}{M_A} - \frac{x_B E_B}{M_B} - \frac{x_C E_C}{M_C} \quad (4)$$

126 where  $M_i$  is the number of molecules in the system,  $E_A$ ,  $E_B$ , and  $E_C$  are the potential energies  
127 of the reference systems (LiF, NaF, and KF),  $E_{ABC}$  is the potential energy of the ternary  
128 system, and  $x_A$ ,  $x_B$ , and  $x_C$  are the mole fraction of the respective reference salts in the  
129 mixture. This same equation can be applied to binary salt mixtures, reducing from four  
130 terms to three. While assumptions can be made to incorporate entropic effects to determine  
131 the free energy of mixing, such a step was not taken due to inherent assumptions required  
132 for ideal solution-type behavior.

133 The binary and unary salt systems were equilibrated in a strictly NPT ensemble, easing  
134 some of the computational burden of exploring varied salt complexes, but limiting the ability  
135 to explore volume-dependent phenomena, such as the compressibility. There are no statis-  
136 tically significant differences in calculated thermodynamic quantities from the utilization of  
137 an NPT versus an NVT ensemble.

### 138 3. Results

#### 139 3.1. Density and Thermal Expansion

140 The density of each composition studied is displayed as a function of temperature in fig. 2.  
141 It should be noted that for all densities reported here, there is an approximate error of 0.05  
142 g/cc. For all compositions, the density decreases with increasing temperature. This is in line  
143 with the inversely proportional relationship between density and temperature. The minimum  
144 density is observed for the pure LiF system, while the maximum density is observed for the  
145 NaF system. All of the densities fall within a range of approximately 0.25 g/cc, with the  
146 intermediate compositions having a much narrower range of only about 0.1 g/cc. Thus, the  
147 maximum variation for the ternary compositions is approximately 5%. All data presented is  
148 also included in tabular form in the appendix.

149 The density can be analyzed by composition, as in fig. 3, where there is an overall decrease in  
150 the density as the percent of LiF increases. The opposite occurs in fig. 3b, where the density  
151 increases as the percent of NaF increases. Looking at fig. 3c, there appears to be little effect as  
152 the percent of KF changes. This seems to be reasonable, as the density of LiF is the lowest, the  
153 density of NaF is the highest, and the density of KF is at an intermediate value between the  
154 other two. It should be emphasized that in fig. 3, ternary, binary, and unary salt densities are  
155 all included. For the three temperatures at which all ten compositions were studied, ternary  
156 heatmaps, shown in fig. 4, were generated to better visualize the effects of the changing  
157 composition. While a limited number of compositions were utilized for the construction of the  
158 ternary density heat maps, they can clearly illustrate the dependence upon the composition.  
159 The composition of the mixture with respect to the LiF-NaF binary system is the primary  
160 determining factor for the density of the ternary, with the KF composition having nearly a  
161 negligible effect. It appears that density decreases more sharply as the composition nears LiF  
162 than the density decreases as the NaF composition increases, but additional data points at

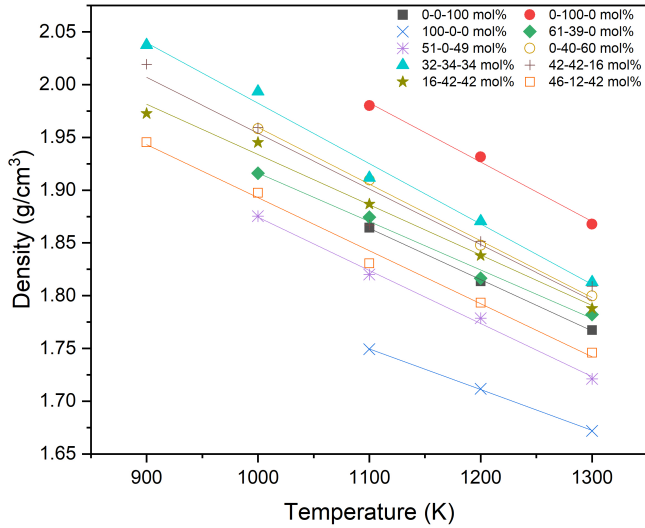


Figure 2: The density ( $\text{g}/\text{cm}^3$ ) versus temperature (K) of all compositions studied (LiF-NaF-KF mol%).

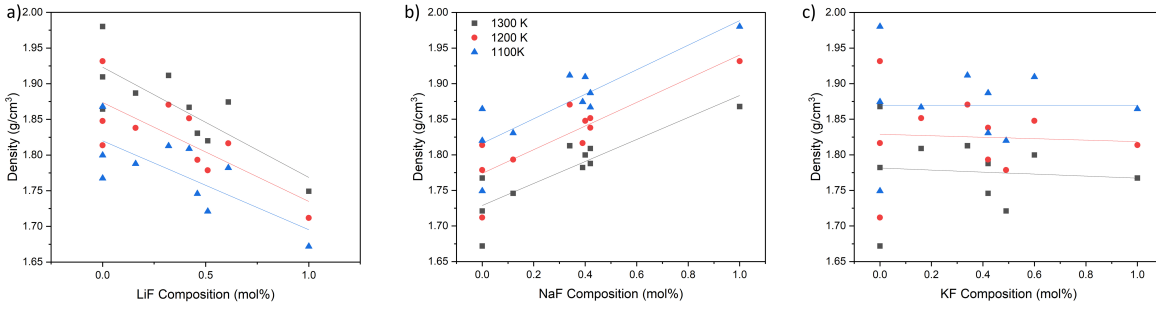


Figure 3: The density ( $\text{g}/\text{cm}^3$ ) as a function of the composition of a) LiF (mol%), b) NaF (mol%), and c) KF (mol%) for different FLiNaK salts.

163 intermediate compositions would be required to verify these behaviors. For the four ternary  
 164 phases, the eutectic is somewhat the outlier, possessing the least NaF and thus exhibiting  
 165 the lowest density. The lower density of the eutectic composition compared to other ternary  
 166 compositions may or may not be preferable. Regardless, these variations are somewhat minor.  
 167 These conclusions hold across the temperature range studied. More complex density surfaces  
 168 may be present but are not identifiable with the limited number of compositions studied here.

169 Experimental densities are available for comparison with the eutectic composition. When  
 170 compared to experimental values from Janz [31] (shown in fig. 5a), this work slightly under-  
 171 predicts the density at all temperatures. The data deviates on average by 0.05 g/cc from  
 172 Janz. For the individual salt endpoints (LiF, NaF, KF), the comparisons with experiments  
 173 are shown in fig. 5b. There is a consistent, but minor, underprediction for the densities at  
 174 all temperatures, but the change in the density with temperature shows good agreement, as  
 175 the average deviation across all individual salts is 0.06 g/cc. As experimental measurements

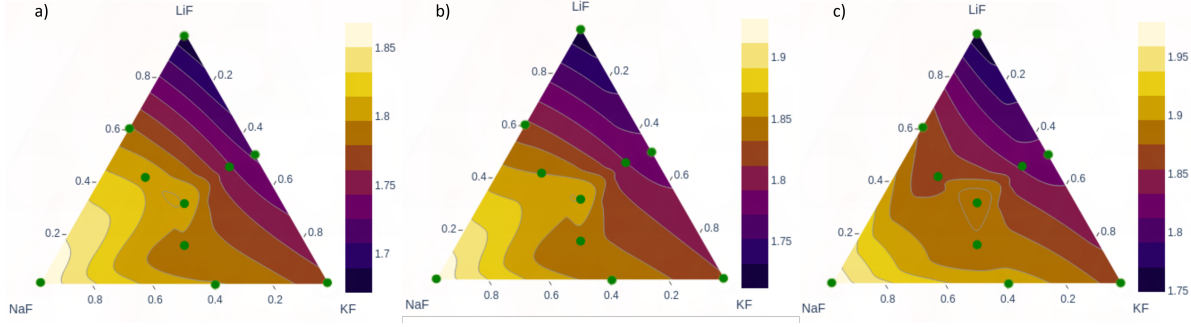


Figure 4: Ternary heatmap of the density ( $\text{cm}^3$ ) of FLiNaK at a) 1300 K, b) 1200 K, and c) 1100 K.

often report uncertainties on the order of 1-5% [32], there is general confidence in the magnitude and trends of the density with varying compositions. The error bars shown in fig. 5 include a 2% error from experiments, and a propagated computational error accounting for the scatter in each individual data point and the error from the quadratic fit, as illustrated in fig. 1. The error bars all predicted densities overlap with the error bars from experiments for all compositions and temperatures.

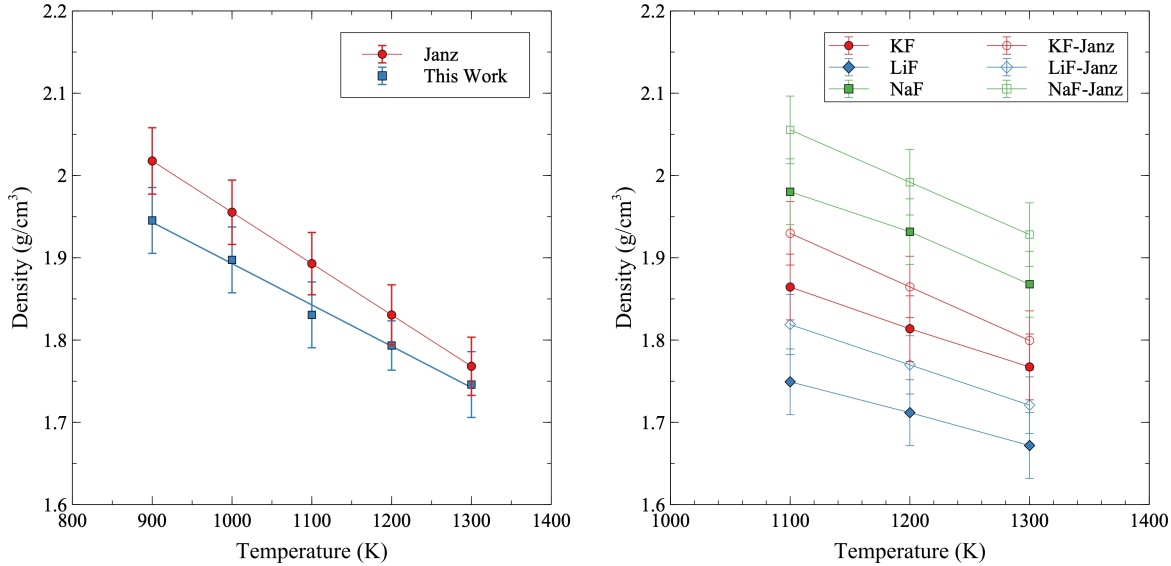


Figure 5: Comparison of density,  $\text{g}/\text{cm}^3$ , versus temperature, K, of a) the eutectic composition with literature[31] and b) pure salts with literature[32].

The thermal expansion can be taken from the slope of the density in fig. 2 with respect to temperature (eq. (3)). The thermal expansion coefficient is plotted versus composition in fig. 6. The trends of the thermal expansion with respect to composition are not as strong as those for density. The LiF concentration in fig. 6a has a negative impact on the coefficient of thermal expansion. However, as shown in fig. 6b and fig. 6c, there is not a statistically significant impact on the thermal expansion of varying compositions of NaF or KF. However, with increasing NaF and KF, there is a minor increase in the thermal expansion. The minimum thermal expansion of the four ternary compositions occurs at 16-42-42 mol %, and

190 the maximum occurs at 32-34-34 mol %. When considering only the ternary compositions,  
 191 the previously stated trends do not apply as there is no statistically significant relationship  
 192 between the composition of the unary salts and thermal expansion.

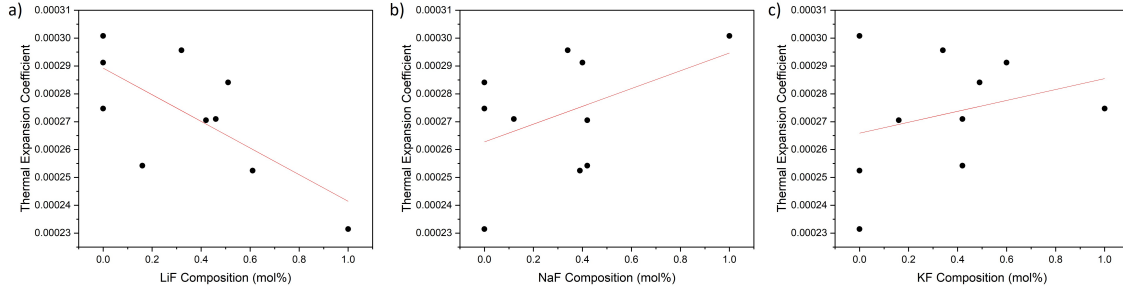


Figure 6: The thermal expansion coefficient versus the composition of a) LiF (mol%), b) KF (mol%), and c) NaF (mol%) for different FLiNaK salts.

### 193 3.2. Bulk Modulus and Compressibility

194 The bulk modulus and the compressibility are shown in fig. 7. It should be emphasized  
 195 that the compressibility is the inverse of the bulk modulus. Both are shown here for com-  
 196 pleteness. The degree of compressibility of a fluid has strong implications for its dynamics.  
 197 As expected, the compressibility increases as the temperature increases. There is significant  
 198 scatter in the data, which makes drawing specific conclusions regarding compositional de-  
 199 pendence difficult, but generally, the eutectic composition has an intermediate value of the  
 200 compressibility. The near equiatomic ternary salt has the lowest compressibility, and the  
 201 low LiF content salt has the highest compressibility. Compared to two binary chloride salts  
 202 (LiCl-KCl [18] and NaCl-MgCl<sub>2</sub> [33]), the ternary compositions of FLiNaK display a lower  
 203 value of the compressibility. Only ternary salts are included here as non-ternary compo-  
 204 sitions were analyzed in an NPT ensemble, which did not allow for the evaluation of the bulk  
 205 modulus.

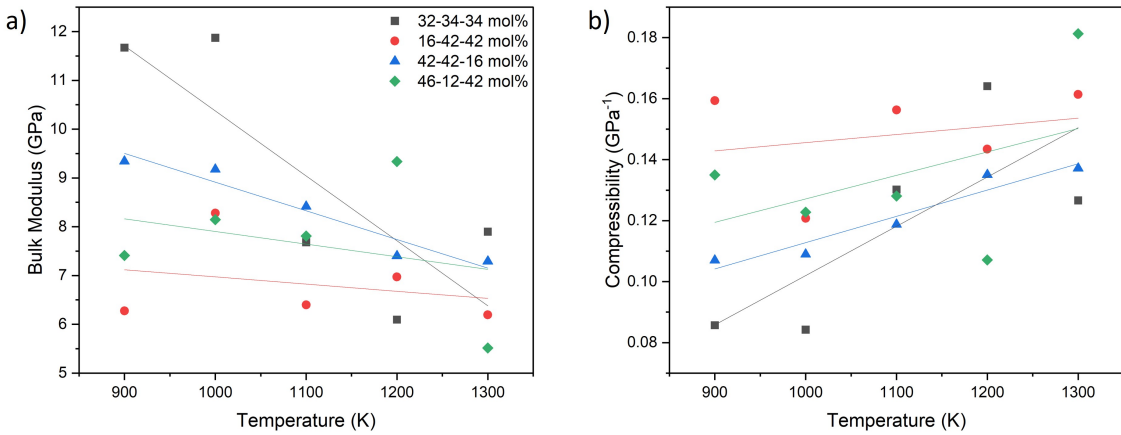


Figure 7: a) Bulk modulus and b) compressibility of the four ternary compositions versus temperature

### 206 3.3. Heat Capacity and Enthalpy of Mixing

207 Heat capacity is a required parameter for thermal hydraulics models describing heat trans-  
 208 port in molten salt systems[3]. The heat capacity for FLiNaK is best visualized as a ternary  
 209 heatmap, shown in fig. 8. The heat capacity is greatest around the middle compositions  
 210 and decreases as the system moves towards the three pure alkali-halide salt constituents. As  
 211 stated, the exact contour locations may vary from their depiction here due to the limited  
 212 number of ternary compositions, but the variance in the heat capacity with composition, in  
 213 that a near equiatomic mixture has the highest heat capacity, is quite consistent. The total  
 214 energy from AIMD simulations shows a linear dependence, thus the heat capacity is effectively  
 215 constant over the investigated temperature range. Williams et al. report the heat capacity  
 216 of the eutectic composition to be 77.9 J/mol-K at 973 K[34], which compares quite favorably  
 217 to the calculated value of 67.6 J/mol-K from this work. Compared to the reported literature  
 218 value, this work underpredicts the heat capacity by 13.2%, but is neglecting the electronic  
 219 contribution to the heat capacity, which, if included, would decrease the discrepancy. This  
 220 is because the total heat capacity is a combination of the electron and phonon contributions  
 221 to the heat capacity [35], and including the electronic component will serve to increase the  
 222 predicted value of the heat capacity. It should be noted that heat capacity measurements  
 223 are notoriously difficult in molten salts, and often are in disagreement with one another [36].  
 224 Generally, a higher heat capacity is preferable for thermal hydraulics applications, and thus  
 225 this work points to a potential benefit of utilizing near-equiatomic compositions of FLiNaK.

226 The enthalpy of mixing is plotted against each of the pure alkali-halide salt constituents  
 227 in fig. 9. Considering that this figure includes both ternary and binary compounds, the char-  
 228 acteristic inverse hull shape is not present. However, intermediate compositions display the  
 229 lowest enthalpy of mixing, with the near-equiatomic (32-34-34) composition exhibiting the  
 230 global lowest energy. Including entropic effects to yield a free energy of formation was beyond  
 231 the scope of this work, but it is anticipated that the near equiatomic composition would likely  
 232 display the largest entropy, and thus the lowest free energy. Unfortunately, there is no exper-  
 233 imental data for comparison. Additionally, prior computational investigations were typically

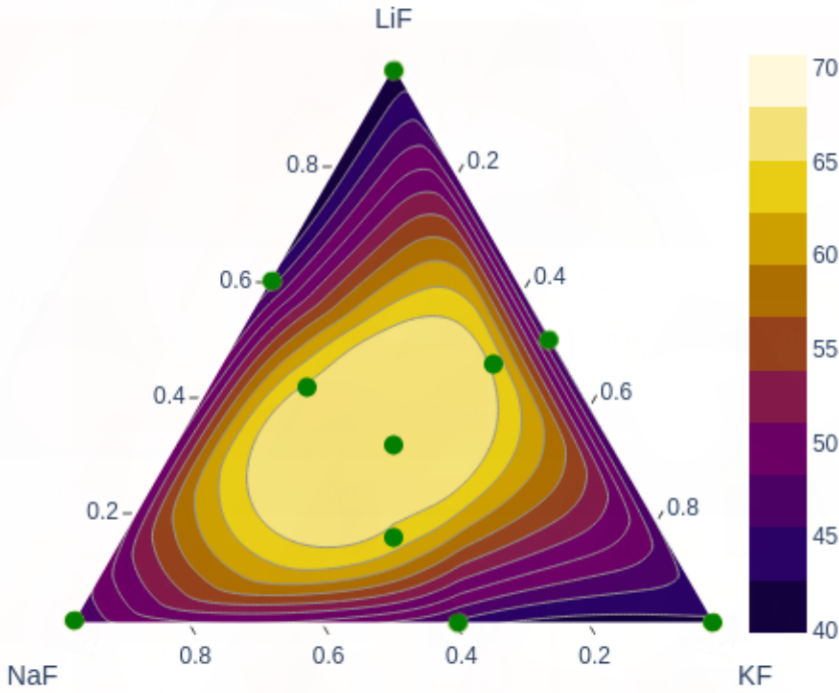


Figure 8: Ternary heatmap of the heat capacity of FLiNaK (J/mol-K).

234 restricted to the eutectic composition and did not explore the unary salt components, which  
 235 prevented them from determining the enthalpy of formation. Experimental and additional  
 236 computational studies are warranted to validate these results.

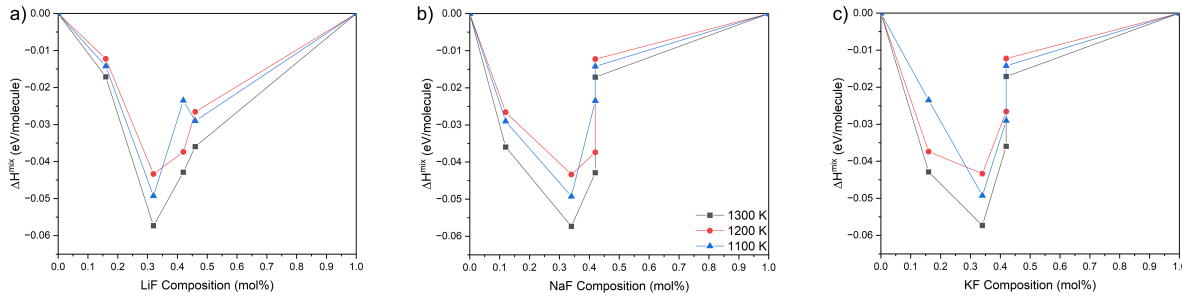


Figure 9: Graph of the enthalpy of mixing, eV/molecule, versus composition of a) LiF (mol%), b) NaF (mol%), and c) KF (mol%).

#### 237 3.4. Coordination Analysis

238 The local atomic structure is analyzed by means of the radial pair distribution function  
 239 (RDF). The RDF, or  $g(r)$ , measures the probability of finding a particle at distance  $r$  given  
 240 that there is a particle at position  $r = 0$ . The peak of the RDF for each pair is the most  
 241 probable location of the first-nearest-neighbor (1nn). The RDF for eutectic LiF-NaF-KF is  
 242 shown in fig. 10 at 900 K. Note that not all pair-wise interactions are shown in fig. 10, to aid

243 in readability. Also, this RDF constitutes a time average over 3 ps of a given simulation at  
 244 the zero-pressure volume at 900 K. The 1nn distance is then determined and compared to  
 245 an x-ray diffraction study conducted at 793 K in table 1. Generally, the RDF compares very  
 246 favorably to the experimental results, as well as a prior computational study [6]. The most  
 247 significant difference being for the F-F peak, which is overestimated by approximately 0.09 Å.  
 248 However, the experimental results assumed a Gaussian distribution for their analysis, which  
 249 may induce small errors, and reported a mean square-root displacement of 0.41 Å, indicating  
 250 a broad peak, which is in accordance with these results and provides additional confidence  
 251 in the accuracy of the simulations. The RDFs of the other ternary systems were analyzed to  
 252 identify potential variations with somewhat minor compositional differences. The individual  
 253 pair distances did not statistically change for the primary species, however, the F-F bond did  
 254 show some variance depending upon the system, with the low Li concentration (16-42-42)  
 255 displaying the longest F-F 1nn distance (3.33 Å) and the eutectic displaying the shortest F-F  
 256 bond 1nn distance (3.14 Å) (table A.3). There is not a clear correlation between F-F 1nn  
 257 distance and density, which one might expect. However, there is a negative linear correlation  
 258 ( $R^2=0.98$ ) with the Li content, with greater Li content exhibiting shorter F-F 1nn distances.  
 259 These minor structural variations would need to be confirmed via experiments and may  
 260 provide insight into dynamical properties related to the distribution of F atoms in FLiNaK  
 261 salts.

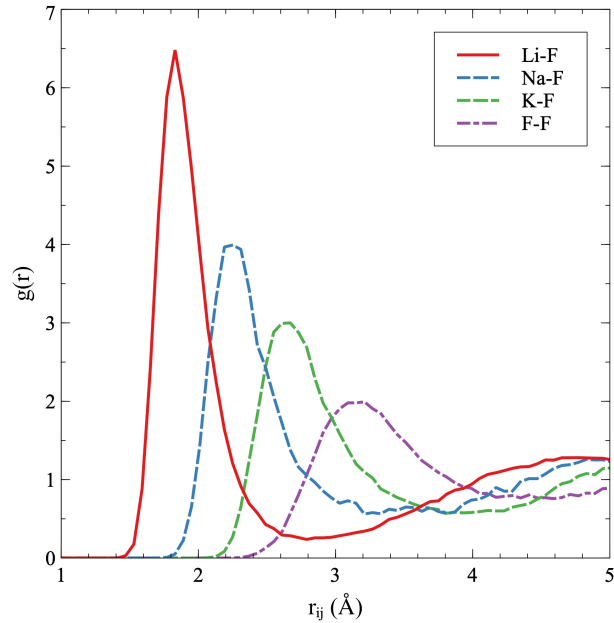


Figure 10: Partial radial distribution functions for eutectic LiF-NaF-KF at 900 K.

Table 1: First nearest neighbor distances for eutectic LiF-NaF-KF at 900 K. Results are compared against experiment at 793 K [37].

Pair	$r_{ij}$ (Å)	$r_{ij}$ (Å)[37]
Li-F	1.82	1.83
Na-F	2.23	2.18
K-F	2.64	2.59
F-F	3.14	3.05

## 262 4. Conclusion

263 To characterize the thermophysical properties of FLiNaK, a first principles computa-  
 264 tional investigation was performed for four ternary compositions, three binary eutectic com-  
 265 positions, and three pure alkali-halide salt constituents. The computational results of the  
 266 density slightly underpredicted the experimental values at all temperatures for the eutectic  
 267 and pure salt compositions. However, generally good agreement is observed. The density  
 268 is positively correlated with the NaF concentration and negatively correlated with the LiF  
 269 concentration. The thermal expansion was determined to decrease with increasing LiF con-  
 270 centration, but there was no statistically significant dependence on NaF or KF. The large  
 271 scatter in the data for the bulk modulus and compressibility resulted in an inability to draw  
 272 specific conclusions about compositional dependence, however, the compressibility increased  
 273 with the temperature, as expected, and displays a magnitude lower than comparable chloride  
 274 salts. The results for the heat capacity, like the density, underpredicted the literature value,  
 275 but are likely within experimental uncertainties. In the enthalpy of mixing versus composi-  
 276 tion, the ternary compositions display the lowest formation energy, with the near equiatomic  
 277 composition possessing the minimum.

278 As the interest in molten salt reactors is renewed, there is a need for thermophysical  
 279 properties of salt systems at varied compositions rather than just the eutectic composition.  
 280 Currently, these properties are largely unknown, but can be elucidated through first principles  
 281 methods. This work has shown that some thermophysical properties can exhibit significant  
 282 differences with relatively minor compositional variance, indicating the potential for tailoring  
 283 even well-known molten salt systems to target specific property behaviors. Further exper-  
 284 imental work is necessary to validate the results presented in this manuscript, providing  
 285 further confidence in the ability of first principles methods to explore the vast composition  
 286 and temperature space relevant to molten salts in nuclear applications.

## 287 5. Acknowledgements

288 This work was supported through the NC State Nuclear Engineering Undergraduate Re-  
 289 search Scholar Program with funding courtesy of the College of Engineering Enhancement  
 290 Fee. This work is also supported through the INL Laboratory Directed Research and Develop-  
 291 ment (LDRD) Program under DOE Idaho Operations Office Contract DE-AC07-05ID14517.  
 292 This research made use of the resources of the High-Performance Computing Center at Idaho  
 293 National Laboratory, which is supported by the Office of Nuclear Energy of the U.S. Depart-  
 294 ment of Energy and the Nuclear Science User Facilities.

<sup>295</sup> Appendix A.

Table A.1: The density ( $\text{g}/\text{cm}^3$ ) of LiF-NaF-KF at different temperatures.

Composition (LiF-NaF-KF)	900 K	1000 K	1100 K	1200 K	1300 K
eutectic 46-12-42	1.95	1.90	1.83	1.79	1.75
16-42-42	1.97	1.95	1.89	1.84	1.79
32-34-34	2.04	1.99	1.91	1.87	1.81
42-42-16	2.02	1.96	1.87	1.85	1.81
0-40-60	-	1.96	1.91	1.85	1.80
51-0-49	-	1.88	1.82	1.78	1.72
61-39-0	-	1.92	1.87	1.82	1.78
100-0-0	-	-	1.75	1.71	1.67
0-100-0	-	-	1.98	1.93	1.87
0-0-100	-	-	1.86	1.81	1.77

Table A.2: The coefficient of thermal expansion ( $\alpha$ ), compressibility ( $\beta$  at 1100 K), heat capacity ( $C_P$ ), and enthalpy of mixing ( $\Delta H_{mix}$  at 1300 K) of LiF-NaF-KF.

Composition (LiF-NaF-KF)	$\alpha \times 10^{-4}$	$\beta (\text{GPa}^{-1})$	$C_P (\text{J/mol-K})$	$\Delta H_{mix}(\text{eV/molecule})$
eutectic 46-12-42	2.88	0.128	67.6	-0.027
16-42-42	2.66	0.121	66.8	-0.017
32-34-34	3.15	0.130	70.7	-0.057
42-42-16	2.93	0.119	68.3	-0.043
0-40-60	2.91	-	43.1	-0.007
51-0-49	2.84	-	43.0	-0.043
61-39-0	2.52	-	42.0	-0.028
100-0-0	2.31	-	39.9	-
0-100-0	3.01	-	44.4	-
0-0-100	2.75	-	41.9	-

Table A.3: The first-nearest-neighbor distances of the ternary LiF-NaF-KF salts at 900K.

Composition (LiF-NaF-KF)	F-F 1nn distance (Å)
eutectic 46-12-42	3.14
16-42-42	3.33
32-34-34	3.21
42-42-16	3.15

## 296 References

- [1] T. Porter, M. Vaka, P. Steenblik, D. Della Corte, Computational methods to simulate molten salt thermophysical properties, *Commun Chem* 5 (2022) 69. doi:10.1038/s42004-022-00684-6.  
 URL <https://www.nature.com/articles/s42004-022-00684-6>
- [2] G. Locatelli, M. Mancini, N. Todeschini, Generation iv nuclear reactors: Current status and future prospects, *Energy Policy* 61 (2013) 1503–1520. doi:10.1016/j.enpol.2013.06.101.  
 URL <https://www.sciencedirect.com/science/article/pii/S0301421513006083>
- [3] Freile, Ramiro, Kimber, Mark, Influence of molten salt-(flinak) thermophysical properties on a heated tube using cfd rans turbulence modeling of an experimental testbed, *EPJ Nuclear Sci. Technol.* 5 (2019) 16. doi:10.1051/epjn/2019027.  
 URL <https://doi.org/10.1051/epjn/2019027>
- [4] O. Beneš, R. Konings, Thermodynamic properties and phase diagrams of fluoride salts for nuclear applications, *Journal of Fluorine Chemistry* (2009) 22–29doi:<https://doi.org/10.1016/j.jfluchem.2008.07.014>.  
 URL <https://www.sciencedirect.com/science/article/pii/S0022113908002030>
- [5] J. Ambrosek, M. Anderson, K. Sridharan, T. Allen, Current status of knowledge of the fluoride salt (flinak) heat transfer, *Nuclear Technology* 165 (2009) 166–173. doi:10.13182/NT165-166.  
 URL <https://www.tandfonline.com/doi/full/10.13182/NT165-166>
- [6] B. A. Frandsen, S. D. Nickerson, A. D. Clark, A. Solano, R. Baral, J. Williams, J. Neufeind, M. Memmott, The structure of molten flinak, *Journal of Nuclear Materials* 537 (2020) 152219. doi:10.1016/j.jnucmat.2020.152219.  
 URL <https://www.sciencedirect.com/science/article/pii/S0022311520304736>
- [7] M. Anderson, K. Sridharan, D. Morgan, P. Peterson, P. Calderoni, R. Scheele, A. Casekka, B. McNamara, Heat transfer salts for nuclear reactor systems - chemistry control, corrosion mitigation, and modeling, Tech. Rep. Project No. 10-905, University of Wisconsin, Madison (1 2015). doi:10.2172/1169921.  
 URL <https://www.osti.gov/biblio/1169921>

- 326 [8] X. Liu, Y. Li, B. Wang, C. Wang, Raman and density functional theory stud-  
327 ies of lutecium fluoride and oxyfluoride structures in molten flinak, Spectrochim-  
328 ica Acta Part A: Molecular and Biomolecular Spectroscopy 251 (2021) 119435.  
329 doi:10.1016/j.saa.2021.119435.  
330 URL <https://www.sciencedirect.com/science/article/pii/S1386142521000111>
- 331 [9] H. W. Hoffman, J. Lones, Fused salt heat transfer. part ii. forced convection heat trans-  
332 fer in circular tubes containing naf-kf-lif eutectic, Tech. Rep. ORNL-1777, Oak Ridge  
333 National Laboratory (2 1955). doi:10.2172/4016896.  
334 URL <https://www.osti.gov/biblio/4016896>
- 335 [10] D. Holcomb, S. Cetiner, An overview of liquid-fluoride-salt heat transport sys-  
336 tems, Tech. Rep. ORNL/TM-2010/156, Oak Ridge National Laboratory (10 2010).  
337 doi:10.2172/990239.
- 338 [11] G. L. Yoder, Jr, D. W. Heatherly, D. F. Williams, Y. M. Elkassabgi, J. Caja, M. Caja,  
339 J. Jordan, R. Salinas, Liquid fluoride salt experimentation using a small natural circu-  
340 lation cell, Tech. Rep. ORNL/TM-2014/56, Oak Ridge National Laboratory (4 2014).  
341 doi:10.2172/1130418.  
342 URL <https://www.osti.gov/biblio/1130418>
- 343 [12] M. Salanne, C. Simon, P. Turq, P. A. Madden, Heat-transport properties of molten  
344 fluorides: Determination from first-principles, Journal of Fluorine Chemistry 130 (2009)  
345 38–44. doi:10.1016/j.jfluchem.2008.07.013.
- 346 [13] S.-C. Lee, Y. Zhai, Z. Li, N. P. Walter, M. Rose, B. J. Heuser, Y. Z, Comparative  
347 studies of the structural and transport properties of molten salt flinak using the machine-  
348 learned neural network and reparametrized classical forcefields, The Journal of Physical  
349 Chemistry B 125 (2021) 10562–10570. doi:10.1021/acs.jpcb.1c05608.  
350 URL <https://pubs.acs.org/doi/10.1021/acs.jpcb.1c05608>
- 351 [14] C. Sona, M. A. Khanwale, C. S. Mathpati, A. Borgohain, N. K. Maheshwari, In-  
352 vestigation of flow and heat characteristics and structure identification of flinak  
353 in pipe using cfd simulations, Applied Thermal Engineering 70 (2014) 451–461.  
354 doi:10.1016/j.applthermaleng.2014.05.043.
- 355 [15] H. Nam, A. Bengtson, K. Vörtler, S. Saha, R. Sakidja, D. Morgan, First-principles  
356 molecular dynamics modeling of the molten fluoride salt with cr solute, Journal of Nu-  
357 clear Materials 449 (2014) 148–157. doi:10.1016/j.jnucmat.2014.03.014.  
358 URL <https://www.sciencedirect.com/science/article/pii/S0022311514001238>
- 359 [16] A. D. Clark, W. L. Lee, A. R. Solano, T. B. Williams, G. S. Meyer, G. J. Tait,  
360 B. C. Battraw, S. D. Nickerson, Complexation of mo in flinak molten salt: Insight  
361 from ab initio molecular dynamics, Journal of Physical Chemistry B 125 (2020).  
362 doi:10.1021/acs.jpcb.0c07354.
- 363 [17] D. Sprouster, G. Zheng, S.-C. Lee, D. Olds, C. Agca, J. McFarlane, Y. Z, B. Khaykovich,  
364 Molecular structure and phase equilibria of molten fluoride salt with and without

- 365 dissolved cesium: Flinak–csf (5 mol %), ACS Applied Energy Materials 5 (2022).  
366 doi:10.1021/acsaem.2c00544.
- 367 [18] K. Duemmler, Y. Lin, M. Woods, T. Karlsson, R. Gakhar, B. Beeler,  
368 Evaluation of thermophysical properties of the licl-kcl system via ab initio  
369 and experimental methods, Journal of Nuclear Materials 559 (2022) 153414.  
370 doi:<https://doi.org/10.1016/j.jnucmat.2021.153414>.  
371 URL <https://www.sciencedirect.com/science/article/pii/S0022311521006346>
- 372 [19] K. Duemmler, M. Woods, T. Karlsson, R. Gakhar, B. Beeler, First-principles-derived  
373 transport properties of molten chloride salts, Journal of Nuclear Materials 585 (2023)  
374 154601. doi:<https://doi.org/10.1016/j.jnucmat.2023.154601>.  
375 URL <https://www.sciencedirect.com/science/article/pii/S0022311523003689>
- 376 [20] D. Zhao, L. Yan, T. Jiang, S. Peng, B. Yue, On the viscosity of molten salts and molten  
377 salt mixtures and its temperature dependence, Journal of Energy Storage 61 (2023)  
378 106707. doi:<https://doi.org/10.1016/j.est.2023.106707>.  
379 URL <https://www.sciencedirect.com/science/article/pii/S2352152X23001044>
- 380 [21] L. Martínez, R. Andrade, E. G. Birgin, J. M. Martínez, Packmol: A  
381 package for building initial configurations for molecular dynamics sim-  
382 ulations, Journal of Computational Chemistry 30 (13) (2009) 2157–  
383 2164. arXiv:<https://onlinelibrary.wiley.com/doi/pdf/10.1002/jcc.21224>,  
384 doi:<https://doi.org/10.1002/jcc.21224>.  
385 URL <https://onlinelibrary.wiley.com/doi/abs/10.1002/jcc.21224>
- 386 [22] A. Bengtson, H. O. Nam, S. Saha, R. Sakidja, D. Morgan, First-principles molecular  
387 dynamics modeling of the licl–kcl molten salt system, Computational Materials Science  
388 83 (2014). doi:10.1016/j.commatsci.2013.10.043.  
389 URL <https://www.sciencedirect.com/science/article/pii/S0927025613006630>
- 390 [23] D. Andersson, B. Beeler, Ab initio molecular dynamics (aimd) simulations of  
391 nacl, ucl3 and nacl-ucl3 molten salts, Journal of Nuclear Materials 568 (2022).  
392 doi:10.1016/j.jnucmat.2022.153836.  
393 URL <https://www.sciencedirect.com/science/article/pii/S0022311522003221>
- 394 [24] G. Kresse, J. Hafner, Ab initio molecular dynamics for liquid metals, Phys. Rev. B 47  
395 (1993) 558–561. doi:10.1103/PhysRevB.47.558.  
396 URL <https://link.aps.org/doi/10.1103/PhysRevB.47.558>
- 397 [25] G. Kresse, J. Furthmüller, Efficiency of ab-initio total energy calculations for metals and  
398 semiconductors using a plane-wave basis set, Computational Materials Science 6 (1996)  
399 15–50. doi:[https://doi.org/10.1016/0927-0256\(96\)00008-0](https://doi.org/10.1016/0927-0256(96)00008-0).  
400 URL <https://www.sciencedirect.com/science/article/pii/0927025696000080>
- 401 [26] G. Kresse, J. Furthmüller, Efficient iterative schemes for ab initio total-energy  
402 calculations using a plane-wave basis set, Phys. Rev. B 54 (1996) 11169–11186.

- 403 doi:10.1103/PhysRevB.54.11169.  
404 URL <https://link.aps.org/doi/10.1103/PhysRevB.54.11169>
- 405 [27] J. Klimeš, D. R. Bowler, A. Michaelides, Chemical accuracy for the van der waals  
406 density functional, *Journal of Physics: Condensed Matter* 22 (2) (2009) 022201.  
407 doi:10.1088/0953-8984/22/2/022201.
- 408 [28] J. Klimeš, D. R. Bowler, A. Michaelides, Van der waals density functionals applied to  
409 solids, *Physical Review B* 83 (19) (may 2011). doi:10.1103/physrevb.83.195131.  
410 URL <https://doi.org/10.1103%2Fphysrevb.83.195131>
- 411 [29] S. Grimme, J. Antony, S. Ehrlich, H. Krieg, A consistent and accurate ab  
412 initio parametrization of density functional dispersion correction (dft-d) for the  
413 94 elements h-pu, *The Journal of Chemical Physics* 132 (15) (2010) 154104.  
414 arXiv:<https://doi.org/10.1063/1.3382344>, doi:10.1063/1.3382344.  
415 URL <https://doi.org/10.1063/1.3382344>
- 416 [30] A. Stukowski, Visualization and analysis of atomistic simulation data with OVITO-the  
417 Open Visualization Tool, *MODELLING AND SIMULATION IN MATERIALS SCI-  
418 ENCE AND ENGINEERING* 18 (1) (JAN 2010). doi:10.1088/0965-0393/18/1/015012.
- 419 [31] G. Janz, R. Tomkins, Physical properties data compilations relevant to energy storage.  
420 iv. molten salts: Data on additional single and multi-component salt systems, *Tech.  
421 Rep. NSRDS-NBS* 61, National Bureau of Standards (1981).
- 422 [32] G. Janz, Thermodynamic and transport properties for molten salts: Correlation equa-  
423 tions for critically evaluated density, surface tension, electrical conductance, and viscos-  
424 ity data, *Journal of Physical and Chemical Reference Data* 17 (1988).
- 425 [33] K. Duemmler, M. Woods, T. Karlsson, R. Gakhar, B. Beeler, An ab  
426 initio molecular dynamics investigation of the thermophysical properties  
427 of molten nacl-mgcl<sub>2</sub>, *Journal of Nuclear Materials* 570 (2022) 153916.  
428 doi:<https://doi.org/10.1016/j.jnucmat.2022.153916>.  
429 URL <https://www.sciencedirect.com/science/article/pii/S0022311522004020>
- 430 [34] D. F. Williams, Assessment of candidate molten salt coolants for the advanced high  
431 temperature reactor (ahtr), *Tech. Rep. ORNL/TM-2006/12*, Oak Ridge National Lab-  
432 oratory (3 2006). doi:10.2172/885975.  
433 URL <https://www.osti.gov/biblio/885975>
- 434 [35] A. Moore, B. Beeler, C. Deo, M. Baskes, M. Okuniewski, Atomistic modeling of high  
435 temperature uranium–zirconium alloy structure and thermodynamics, *Journal of Nu-  
436 clear Materials* 467 (2015) 802–819. doi:<https://doi.org/10.1016/j.jnucmat.2015.10.016>.  
437 URL <https://www.sciencedirect.com/science/article/pii/S0022311515302683>
- 438 [36] S. G. Robertson, R. Wiser, W. Yang, D. Kang, S. Choi, E. Baglietto, M. P. Short, The  
439 curious temperature dependence of fluoride molten salt thermal conductivity, *Journal of*

- 440 Applied Physics 131 (22), 225102 (06 2022). arXiv:[https://pubs.aip.org/aip/jap/article-pdf/doi/10.1063/5.0088059/16508374/225102\\_1\\_online.pdf](https://pubs.aip.org/aip/jap/article-pdf/doi/10.1063/5.0088059/16508374/225102_1_online.pdf), doi:10.1063/5.0088059.  
441  
442 URL <https://doi.org/10.1063/5.0088059>
- 443 [37] K. Igarashi, Y. Okamoto, J. Mochinaga, H. Ohno, X-ray diffraction study of molten  
444 eutectic lif–naf–kf mixture, J. Chem. Soc., Faraday Trans. 1 84 (1988) 4407–4415.  
445 doi:10.1039/F19888404407.  
446 URL <http://dx.doi.org/10.1039/F19888404407>